Tuning the spontaneous light emission in phoxonic cavities

Evangelos Almpanis,[1,*] Nikolaos Papanikolaou,[1] Georgios Gantzounis,[2] and Nikolaos Stefanou[3]

[1]*Department of Microelectronics, Institute of Advanced Materials, Physicochemical Processes, Nanotechnology and Microsystems, NCSR " Demokritos," GR-153 10 Athens, Greece*
[2]*Graduate Aeronautical Laboratories (GALCIT) and Department of Applied Physics, California Institute of Technology, Pasadena, California 91125, USA*
[3]*Section of Solid State Physics, University of Athens, Panepistimioupolis, GR-157 84 Athens, Greece*
**Corresponding author: almpanis@imel.demokritos.gr*

Received June 14, 2012; revised July 17, 2012; accepted July 19, 2012;
posted July 20, 2012 (Doc. ID 170614); published August 30, 2012

The modulation of spontaneous light emission of active centers through elastic waves in Si/SiO_2 multilayer phoxonic structures that support dual photonic-phononic localized modes, in the bulk or at the surface, is studied by means of rigorous full electrodynamic and elastodynamic calculations. Our results show that strong dynamic modulation of the spontaneous emission can be achieved through an enhanced acousto-optic interaction when light and elastic energy are simultaneously localized in the same region. © 2012 Optical Society of America

OCIS codes: 230.1040, 260.3800, 230.4170.

1. INTRODUCTION

It has long been recognized that the spontaneous emission of an excited atom is not an inherent property of the atom but also depends on its environment, since the latter can drastically alter the vacuum fields that drive the excited atom to its ground state. It was first suggested by Purcell [1] that the spontaneous emission rate associated to nuclear magnetic moment transitions at radio frequencies can be increased by many orders of magnitude if the system is coupled to an electromagnetic (EM) resonator. In this respect, enhanced spontaneous emission has been demonstrated inside dielectric multilayer microcavities [2–7], slabs [8], dielectric particles [9], and waveguides [10,11].

The theory of spontaneous emission in photonic structures has been elaborated by many authors in both classical [12] and quantum [13,14] regimes. In the classical regime of weak coupling between the EM field and the emitter, the spontaneous emission rate can be evaluated using classical electrodynamics, in conjunction with Fermi golden rule, and turns out to be proportional to the photonic projected local density of states. In this context, light emission in one-dimensional dielectric layered structures can be described theoretically by means of simple transfer-matrix calculations [6]. A detailed classical and quantum mechanical analysis of spontaneous emission in lossless multilayer dielectric structures was recently reported for dipole emitters in silicon waveguides and simple silicon/air structures [13]. Moreover, similar theoretical studies in silicon slot waveguides [15] provide evidence for strong spontaneous emission enhancement over a broad frequency range in appropriately designed structures.

The influence of a time-varying environment on light emission has lately drawn increasing attention due to the development of advanced experimental techniques. Electro-optic [16] and thermo-optic [17] tuning have already been demonstrated. In addition, dynamic tuning of light emission from a single quantum dot inside a nanocavity in a photonic crystal was also recently reported [18]. In that study, coherent acoustic phonons with frequencies of a few gigahertz, formed by a surface acoustic wave, were used to trigger mechanical vibrations and modify the geometry of the cavity. These vibrations cause a periodic modulation of the photonic cavity, which influences fluorescence. Moreover, Brüggemann *et al.* [19] studied the influence of strain pulses on the photoluminescence spectra of InGaAs quantum dots in a λ-cavity of a GaAs layer sandwiched between two GaAs/AlAs Bragg mirrors and found that a strain pulse can enhance the light emission intensity from a random distribution of quantum dots, since shaking brings nominally off resonant quantum dots into the frequency window appropriate for coupling to the cavity mode. Similarly, there are attempts to control light emission with elastic and surface acoustic waves [20–23] by taking advantage of the influence of an elastic field on the dynamics of excitons in multilayer semiconductor cavities or quantum dots through the effect of strain on the electronic band structure.

Recently, there is a growing interest on dynamic photonic structures, controlled by elastic waves, and consequent phenomena [24–32]. Elastic waves can change the geometry and refractive index of a photonic cavity, and thus modify its optical properties. The interplay between optical and elastic waves is exploited in the emerging field of cavity optomechanics, where the optical pressure of localized light in a cavity produces an elastic wave through mechanical deformation [28–30]. Additionally, it has been shown that appropriately designed cavities that support simultaneously photonic and phononic localized resonant modes, so-called phoxonic cavities, allow for strong nonlinear acousto-optic (AO) interactions, which can lead to enhanced modulation of light by acoustic waves through multiphonon exchange mechanisms [31,32].

In this paper, we report a thorough investigation of spontaneous emission in multilayer phoxonic cavities and focus on

the influence of an elastic wave, which resonantly vibrates the cavity region, on the emission rates, based on rigorous full electrodynamic and elastodynamic calculations. Our description is valid for light–matter interaction in the weak coupling regime. For systems with quantum wells or quantum dots, it has been reported that elastic waves influence the quantum efficiency by modulating the electron band structure and the exciton wavefunctions of the emitter [19,33]. However, here, we shall be concerned only with the influence of the photonic environment, modulated by an elastic wave, ignoring modifications of the electron states due to pressure variations. Therefore, we consider fast emitters and elastic waves of frequency much smaller than the spontaneous emission rate, in which case the effect of the elastic wave occurs, mainly, through the modulation of the refractive index and the interfaces of the photonic environment. Our approach is a first step towards the description of a dynamically tuned elastic-wave-driven light emission.

Two different cases are elaborated in detail: (i) a cavity structure where optical and elastic energy is localized in a defect layer between two Bragg mirrors and allows for an enhanced AO modulation of light that escapes the cavity, and (ii) an appropriately engineered surface that sustains simultaneously surface-localized states for both optical and elastic waves and allows for a strong modulation of light that couples to guided modes trapped in the multilayer. Our calculations are based on the layer-multiple-scattering method, which is well documented for both electrodynamics and elastodynamics [34–36]. This method constitutes a powerful tool for an accurate description of the optical and the acoustic response of composite structures comprised of a number of different layers having the same two-dimensional periodicity in the x-y plane (parallel to the layers). For each layer, the method calculates the appropriate transmission and reflection matrices $\mathbf{Q}^{\mathrm{I}}$ and $\mathbf{Q}^{\mathrm{III}}$, respectively, for a plane wave of given angular frequency, ω, incident on the layer with given x-y component of the wave vector, $\mathbf{q}_{\parallel}$, from $z \to -\infty$, as well as the corresponding matrices $\mathbf{Q}^{\mathrm{IV}}$ and $\mathbf{Q}^{\mathrm{II}}$ for incidence from $z \to +\infty$. Explicit expressions for these Q matrices can be found elsewhere [34,36]. The transmission and reflection matrices of the composite structure are calculated from those of the constituent layers. We note that, in the cases considered here, we deal with the simple situation where all layers are homogeneous.

2. A DEFECT LAYER BETWEEN TWO SI/SIO$_2$ MULTILAYER BRAGG MIRRORS

Before going into the resonant elastic-wave-modulated emission, to facilitate the understanding of the different cases presented below, we briefly discuss light emission of an active center implanted into an unperturbed multilayer structure. We consider a SiO_2 defect layer, sandwiched between two multilayer Bragg mirrors, embedded in a SiO_2 matrix. Each Bragg mirror consists of five periods of alternating Si and SiO_2 layers, of thickness $a/3$ and $2a/3$, respectively. The structure is schematically presented in Fig. 1(a). A constant refractive index is assumed for both SiO_2 ($n_{SiO_2} = 1.46$) and Si ($n_{Si} = 3.46$). The two Bragg mirrors on the left and right of the defect layer cause localization of optical modes. The quality factor of this cavity can be increased by using Bragg mirrors with more Si/SiO_2 periods and is only limited by possible

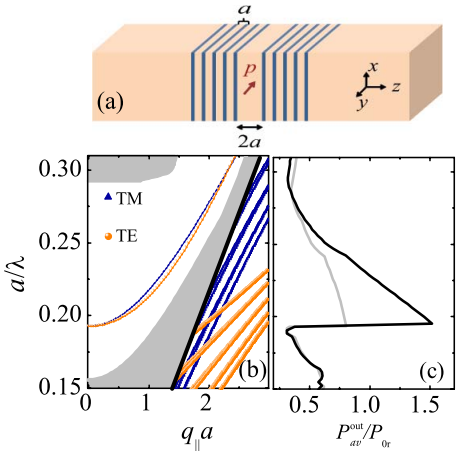

Fig. 1. (Color online) (a) Schematic view of a one-dimensional Si/SiO_2 multilayer cavity. A dipole emitter is placed in a SiO_2 defect layer, of thickness $2a$. Five periods of alternating Si (thickness $a/3$) and SiO_2 (thickness $2a/3$) layers, on both sides of the defect, act as Bragg mirrors for both photons and phonons and create a phoxonic cavity. (b) Photonic dispersion diagram of the structure of (a). The thick straight line is the light line in SiO_2. Above the light line, white areas indicate gap regions over which transmission is vanishingly small, and gray regions correspond to finite transmission, while a transmittance close to unity is calculated for the cavity modes. Below the light line, we display the dispersion diagram of the slab eigenmodes. (c) Average normalized power emitted away from the multilayer slab shown in (a) in the SiO_2 host, for a dipole emitter placed at the center of the defect layer (black line) and at a distance $\Delta z = a/2$ away from the center (gray line).

fabrication imperfections and absorption losses. In Figs. 1(b) and 1(c), we show the calculated dispersion diagram of the photonic modes of the given multilayer slab, together with the normalized emitted power by a radiating dipole placed in the middle of the defect layer, with a random orientation of its dipole moment. This is calculated by integrating over two planes on the left and right of the multilayer structure (see appendix).

Generally, in multilayer structures, because of their invariance parallel to the layers, the modes of the EM field can be classified into transverse electric (TE), if the electric field oscillates parallel to the interfaces, and transverse magnetic (TM), if the magnetic field oscillates parallel to the interfaces. Above the light line, defined by $q_{\parallel} = n_{SiO_2}\omega/c$, the modes are propagating in the SiO_2 host and can be excited by an externally incident plane wave of the appropriate polarization (s or p for the TE or TM modes, respectively) and corresponding $q_{\parallel}$. The gray-shaded areas in Fig. 1(b) correspond to high optical transmission, and the white areas denote negligibly small transmission. The cavity induces a sharp resonance in the transmittance inside the forbidden frequency region created by the Bragg mirrors. This cavity mode, for $q_{\parallel} = 0$ where the TE and TM modes are degenerate, has a quality factor $Q = 1750$ and appears at $a/\lambda = 0.19287$, which corresponds to a wavelength $\lambda = 1.55$ μm by choosing $a = 300$ nm. For $q_{\parallel} \neq 0$, the TE–TM degeneracy is lifted and the TE modes are slightly below the TM modes. The cavity eigenfrequencies move higher with increasing $q_{\parallel}$ and are merged into the continuous spectrum of the system eigenmodes. The cavity modes have a relatively strong field intensity in the central SiO_2 region with a peak in the middle of the defect layer. Below the light line, all modes are guided and decay exponentially outside the multilayer slab, on either side of it. These

modes cannot be excited by an externally incident wave because they cannot match continuously a propagating mode of the EM field outside the slab; momentum and energy cannot be conserved simultaneously. The TE modes are mainly concentrated in the high-refractive-index Si regions, and this is consistent with the lower group velocity of these modes, which approach the Si light line for larger $q_{\parallel}$ values.

Strong light localization in the defect layer with efficient coupling to light travelling outside the multilayer slab is achieved by the cavity mode. Our calculations show a sharp increase of the emitted power at the bottom of the defect band, for $q_{\parallel} = 0$, where the flatness of the band indicates a high density of states. This increase does not depend critically on the exact position of the dipole. Placing for example the dipole at $\Delta z = a/2$ from the center of the defect layer causes only a reduction of the peak of the emitted power, as shown in Fig. 1(c). Therefore, for any distribution of randomly oriented dipoles inside the defect layer, a sharp increase of the emitted power is expected at the onset of the defect band. Our results show that the abrupt increase of the emitted power at the onset of the defect band is due to dipoles oscillating parallel to the interfaces, while the outgoing light is strongly suppressed for a dipole oscillating normal to the slab interfaces since, in this case, $\hat{\mathbf{e}}_2 \cdot \hat{\mathbf{p}}_d = 0$ and the emitted light couples only to TM modes [see Eq. (A6) in the appendix].

The effect of an elastic wave on the optical response of a multilayer cavity was studied previously [31,32]. The main conclusion was that the AO interaction between simultaneously resonant optical and elastic fields could be enhanced by an order of magnitude compared to a nonresonant elastic excitation. This increases the probability for multiphonon exchange mechanisms and leads to larger amplitude modulation of the optical spectra. The effect should be clearly observable for high-Q optical resonances. An elastic wave with submicrometer wavelength can be generated by heating a thin metallic film on the one side of the sample with a femtosecond laser pulse. As a consequence, a broadband elastic wave is generated following the thermal expansion of the metal. For example, using Au films, waves with frequencies up to few tens of gigahertz can be produced [19].

The elastic transmission spectrum for a compressional wave incident normally on the multilayer structure of Fig. 1(a) is displayed in Fig. 2(a). In the calculations, we used a mass density $\rho = 2.20(2.33)$ g/cm^3 and a longitudinal sound velocity $c_l = 5970(8430)$ m/s for SiO_2 (Si). By choosing the lattice constant of the Bragg mirrors $a = 300$ nm, a gap appears for compressional elastic waves between 9.5 and 12.5 GHz, while elastic energy is localized inside the SiO_2 defect layer at a frequency $\Omega/2\pi = 10.98$ GHz. The displacement amplitude profile, associated with this defect mode, is depicted in Fig. 2(b), together with the corresponding strain field [Fig. 2(c)]. At the acoustic resonance frequency and for an input strain level of about 10^{-3}, we obtain a strain level inside the cavity that does not exceed $6 \cdot 10^{-3}$. We note that similar values for the strain in multilayers are reported in recent experiments [19]. It is worth noting that elastic waves cannot be strongly localized in cavities without significant absorption and high-Q factors are not easily achieved.

We follow the approach, described in [31], to calculate the influence of a compressional elastic wave on the spontaneous emission in the structure under consideration. We assume

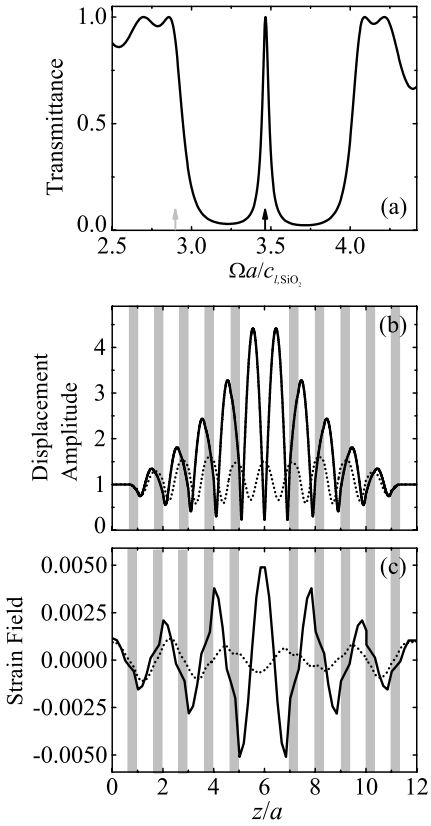

Fig. 2. (a) Transmission spectrum of a compressional elastic wave incident normally on the multilayer structure of Fig. 1(a). (b) Displacement amplitude profile, normalized to the input displacement level, at the resonance frequency $\Omega_{on} = 3.466 c_{l,SiO_2}/a$ (solid line) and at an off-resonance frequency $\Omega_{off} = 2.857 c_{l,SiO_2}/a$ (dotted line), indicated by the arrows in (a). (c) A snapshot of the corresponding strain fields.

an isotropic AO coefficient, $p = 0.22$, for SiO_2 and ignore the AO coefficient of Si, which is rather small. The layers are subdivided into a large number of elementary sublayers and a uniform refractive index change is calculated for each sublayer, due to the compressional elastic wave, by $\Delta n_i = -1/2 p_i n_i^3 S_i$, where n_i and S_i are the average refractive index and strain in sublayer i. Both the material-dependent, so-called bulk, AO effect as well as the influence of the moving interfaces (so-called interface AO effect) are included in the calculations. The choice of a resonant elastic perturbation has been made because it induces a more pronounced dynamic modulation of the optical parameters of the structure, through an enhanced AO interaction, compared to the nonresonant case. The overall spectral features of the photonic dispersion diagram do not change much as time evolves, whereas the position of the optical cavity modes oscillates with an amplitude $\Delta\omega/\omega = 10^{-3}$ at the driving frequency of the resonant elastic excitation. This effect can be understood as follows. Assuming that the elastic wave does not affect drastically the structure under study so that both photonic band gap and cavity modes are maintained, the induced periodic variation of the refractive index and thickness of the defect layer results in a periodic oscillation of the position of the optical cavity modes in the gap with the same period. If both optical and acoustic cavity modes are involved, their interaction is enhanced because of the simultaneous concentration of the respective fields for a long time period in the defect region. In the wave picture, this is manifested as a large-amplitude

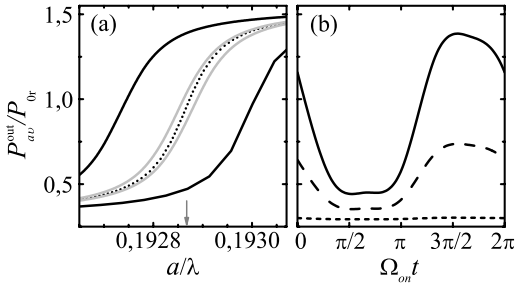

Fig. 3. (a) Modulation of the average normalized power, emitted away from the multilayer slab of Fig. 1(a) in the SiO_2 host by a dipole emitter placed at the center of the defect layer, under elastic excitation at two different frequencies. The dotted line corresponds to the static case and is a zoom of Fig. 1(c), while the solid lines correspond to snapshots under the influence of the elastic field at which maximum changes are obtained. Black line: elastic wave at resonance. Gray line: elastic wave off-resonance (see Fig. 2). (b) Temporal variation of the emitted light power at $a/\lambda = 0.19287$ over a period of the resonant elastic excitation for a randomly oriented dipole at three different positions in the SiO_2 defect layer: at the center (solid line), at a distance $\Delta z = a/2$ from the center (dashed line), and at a distance $\Delta z = a$ from the center, i.e., at the defect layer surface (short-dash line).

oscillation of the position of the optical resonance [31]. The corresponding emitted power outside the multilayer slab for an emitter implanted in the middle of the defect layer, averaged over all dipole orientations, is displayed in Fig. 3(a) for two different acoustic frequencies, one on- and one off-resonance. Here, it can be seen that the resonant AO interaction strongly modulates, also, the emitted light power outside the slab so that, for example, at $a/\lambda = 0.19287$, we periodically switch from enhanced to reduced spontaneous emission. This switching is not possible for elastic excitations off-resonance where only a small modulation is predicted. The temporal variation (within one period of the resonant elastic wave) of the emitted light power for parallel dipoles at different positions in the central SiO_2 defect layer is shown in Fig. 3(b). The emitted power is maximum for a dipole in the middle of the defect layer and is reduced as we approach its surfaces. The amplitude of the AO modulation is also maximum in the middle of the defect layer [see Fig. 2(c)], but also dipoles away from the center emit in phase as shown in Fig. 3(b). It is also to be noted that, for dipoles close to the SiO_2 cavity surfaces, light emission is small and is almost insensitive to the elastic wave.

3. SI/SIO$_2$/SI SLOT WAVEGUIDE ON TOP OF A BRAGG MIRROR

In the multilayer structure considered in the previous section, the cavity mode does not influence appreciably the light that couples to slab eigenmodes and is guided parallel to the slab. By design, at the resonance frequency, the cavity allows more light to escape the structure and suppresses emission into slab modes. In general, light emission can be tailored by adjusting the coupling of the emitted light to different modes of the structure. For example, by reducing the thickness of the SiO_2 defect layer, it is possible to funnel the emitted power into slab-guided modes so that the power escaping the multilayer slab is minimized. If the SiO_2 defect layer becomes very thin, the electric field associated with the cavity mode shows a minimum in the middle of the structure and maxima in the Si layers closer to the defect layer. This leads to efficient coupling of the emitted power of a normal dipole to slab-guided modes. Such Si/SiO_2/Si slot waveguides have been studied previously by Jun *et al.* [15], and our results confirm the main conclusions of that work, namely a strong broadband enhancement of the power coupled to guided modes of the slab. To achieve efficient AO modulation, however, optical and elastic fields should be made resonant, simultaneously, in the same region in space. For this purpose, we consider the multilayer stack shown in Fig. 4(a), which consists of a Si($a/12$)/SiO_2($a/60$)/Si($a/12$)/SiO_2(a)/Si($a/3$) slot waveguide structure (the respective layer thickness is given in parenthesis) on top of a nine-period SiO_2($2a/3$)/Si($a/3$) Bragg mirror on a SiO_2 substrate. The structure is designed to simultaneously support an optical surface state and a longitudinal elastic mode localized close to the surface, which, if driven simultaneously on-resonance, should induce strong, resonant AO interaction.

The dispersion diagram of the guided optical modes of the structure are presented in Fig. 4(b). Because of the different terminations (air and SiO_2), only modes that are below the SiO_2 light line are trapped in the multilayer. Terminating the Si/SiO_2 periodic structure with the Si slot waveguide results in an optical guided mode that appears close to the light line above $a/\lambda = 0.43035$. Our analysis shows that this mode is localized close to the surface in the slot waveguide and for a significant $q_{\parallel}$ range it is the only state available below the light line in this frequency region. For a dipole inside the thin SiO_2 layer of the Si slot waveguide, oscillating normal to the multilayer interfaces, the existence of this surface-localized state leads to a sharp rise of the emitted light that couples to the slab modes as shown in Fig. 4(c). Contrary to the case of the cavity between two Bragg mirrors studied in the previous section, here, the parallel dipoles have low emission, with very small variation in the spectral region of the surface state. The photonic environment of the slot waveguide favors more efficient emission from normal dipoles. It is worth not-

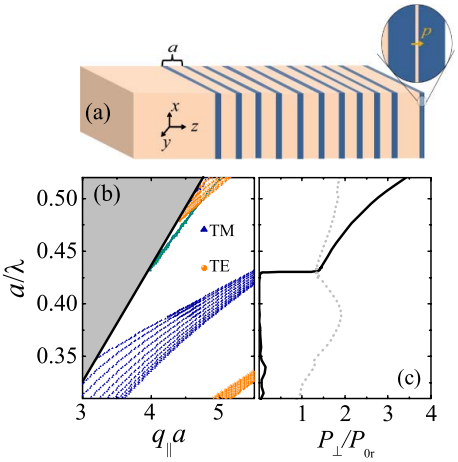

Fig. 4. (Color online) (a) Schematic view of a Si/SiO_2 multilayer slab with a slot waveguide structure on top of a nine-period Bragg mirror (for the geometrical parameters see text) on a SiO_2 substrate. (b) Photonic dispersion diagram of the structure of (a). The thick straight line is the light line in SiO_2. The TM surface state is indicated with the green color. (c) Normalized power emitted away from the multilayer slab of (a) in the SiO_2 host and air (gray dotted line) and trapped into the slot waveguide (black line), for a normal dipole emitter placed at the center of the thin SiO_2 layer in the slot waveguide.

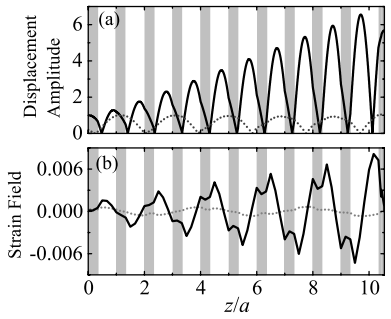

Fig. 5. A compressional elastic wave is incident normal to the multilayer structure of Fig. 4(a) from the SiO_2 substrate. (a) Displacement amplitude profile, normalized to the input displacement level, at the resonance frequency $\Omega_{on} = 4.005 c_{l,SiO_2}/a$ (solid line) and at an off-resonance, frequency $\Omega_{off} = 1.878 c_{l,SiO_2}/a$ (dotted line). (b) A snapshot of the corresponding strain fields.

ing that the emission enhancement to guided modes increases as we move to higher frequencies above the mode cutoff (not shown here). We have actually reproduced the results of previous studies [15], where it was demonstrated that a greater than tenfold enhancement in the spontaneous emission can be achieved.

Elastically the structure behaves as a cavity with the Bragg mirror on one side and an almost total reflector on the other due to the large elastic impedance mismatch between air and the solid material. This geometry supports surface resonances that can be excited by a compressional elastic wave incident from the homogeneous SiO_2 substrate. In Fig. 5, we depict the displacement amplitude profile and strain field for two acoustic frequencies, one on- and one off-resonance. The resonance frequency is inside the elastic band gap of the Si/SiO_2 periodic structure [see Fig. 2(a)]. At this frequency, displacement and strain are maximized as we move closer to the free surface. Strain is significant in the Si regions but, due to the zero AO coefficient assumed for Si, the AO effect is here mainly due to the presence of the free surface that allows for larger amplitude modulation of the interfaces.

The influence of the elastic wave on the optical power emitted to slab modes for frequencies close to the optical surface state is shown in Fig. 6. In the time domain, the emission spectra oscillate in frequency and we depict snapshots of the

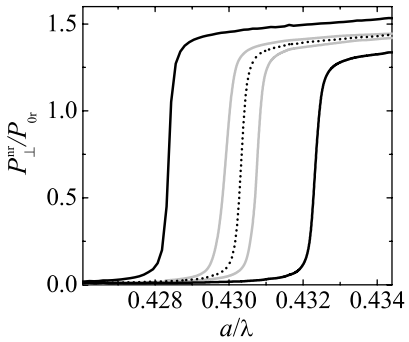

Fig. 6. Modulation of the normalized power, trapped by the surface mode [$P_{\perp}^{nr}$: second term of Eq. (A11)] of the multilayer slab of Fig. 4(a) for a normal dipole emitter at the center of the thin SiO_2 layer, under elastic excitation at two different frequencies. The dotted line corresponds to the static case and is a zoom of Fig. 4(c), while the solid lines correspond to snapshots under the influence of the elastic field at which maximum changes are obtained. Black line: elastic wave at resonance. Gray line: elastic wave off-resonance (see Fig. 5).

time-varying emitted power that yield the maximum changes. These changes of course depend on the frequency of the elastic wave. For the resonant elastic excitation, we find a much larger shift of the emitted power compared with an elastic excitation off resonance.

Similar to the cavity structure studied in the previous section, resonant AO interaction could achieve a modulated emission using moderate and experimentally accessible input strains. Moreover, the modulation amplitude achieved with the surface-localized waves is an order of magnitude larger compared to that in the cavity in the bulk structure, discussed in the previous section, for the same input strain. However, it should be noted that, in the present case, the optical mode involved appears at higher frequencies and, in order for our assumption of $n_{Si} = 3.46$ to be valid, the photon energy must be smaller than the Si band gap, which implies a Bragg stack period a larger than about 500 nm. Alternative materials, such as silicon nitride or TiO_2, could be used in the place of Si to engineer tunable emission also in the visible range.

4. CONCLUSIONS

In summary, we presented a theoretical study of light emission, in the weak light–matter interaction regime, in Si/SiO_2 multilayer structures that support localized resonant modes for both optical and elastic waves. Our results provide evidence for strong dynamic modulation of spontaneous emission about the sharp edge of the optical resonant mode, under the influence of an external elastic wave that excites the elastic resonant mode and induces an enhanced AO interaction. We have considered structures that modulate both light coupled to slab-guided modes and light that escapes the multilayer. Our work is a first step towards the understanding of light emission in time-varying photonic environments and, more specifically, in phoxonic cavities where, because of the resonant character of the fields, strong AO effects take place.

APPENDIX A: CALCULATION OF SPONTANEOUS EMISSION RATES IN MULTILAYERS

In this appendix, we present in some detail the theoretical method for the calculation of spontaneous emission rates of an elementary emitter in a multilayer structure, in the framework of classical electrodynamics. We consider a sequence of different homogeneous layers, stacked along the z direction, and an elementary emitter located at point $\mathbf{r}_d$ inside the multilayer stack. Because of the invariance of the system parallel to the layers, the x-y component, $\mathbf{q}_{\|}$, of the wave vector $\mathbf{q}$ of a plane EM wave propagating through this structure remains constant. The response of each layer to a plane EM wave incident with given $\mathbf{q}_{\|}$ and angular frequency ω is described by appropriate 2×2 transmission and reflection matrices [37]. In conformity with the layer-multiple-scattering method [34,35], we denote these matrices, respectively, by $\mathbf{Q}^{I}$ and $\mathbf{Q}^{III}$ for incidence from the left ($z \to -\infty$) and $\mathbf{Q}^{II}$ and $\mathbf{Q}^{IV}$ for incidence from the right ($z \to \infty$). These matrices are diagonal in the basis of linear-polarization modes where the electric field oscillates in the plane of incidence (p polarization) and normal to this plane, i.e., parallel to the layers (s polarization). We denote the corresponding polarization vectors by $\hat{\mathbf{e}}_1(\mathbf{q})$ and $\hat{\mathbf{e}}_2(\mathbf{q})$, which are the polar and azimuthal

unit vectors, respectively, associated with the given direction of propagation $\mathbf{q}$ and are perpendicular to $\mathbf{q}$. The transmission and reflection matrices of a multilayer stack can be evaluated from those of the constituent layers in the spirit of the layer-multiple-scattering method [34,35] and retain their diagonal form in the given basis: $Q_{pp'} = Q_p \delta_{pp'}$, $p, p' = 1, 2$.

Let us first consider what happens if the system under consideration is illuminated by a monochromatic EM wave of angular frequency ω with electric-field component given by $\mathbf{E}(\mathbf{r}, t) = \mathrm{Re}[\mathbf{E}(\mathbf{r}) \exp(-i\omega t)]$. In the long-wavelength approximation (the optical and infrared wavelengths are typically three orders of magnitude larger than the dimensions of the emitter), the interaction between the emitter and the external field is described by the Hamiltonian $\hat{H}_{\mathrm{int}} = -\hat{\mathbf{p}}_d \cdot \hat{\mathbf{E}}$, i.e., a coupling term between the electric dipole moment of the emitter and the external electric field. According to Fermi golden rule, the excitation rate is proportional to the squared magnitude of the matrix element of $\hat{H}_{\mathrm{int}}$ between the initial and the final states. In the absence of any objects in the environment, the emitter is excited by the incident radiation field $\mathbf{E}_{\mathrm{in}}$. Scattering by the structured environment gives rise to a secondary wave, so that the total field $\mathbf{E}$ is composed by the primary plus the secondary field. We assume that the environment affects the local exciting field and the emitted radiation but not the molecular transitions. The emitter is treated as a classical electric dipole at point $\mathbf{r}_d$ with electric dipole moment $\mathbf{p}_d$. In the regime below saturation, the excitation rate is enhanced by a factor $\eta_{\mathrm{exc}} = |\mathbf{p}_d \cdot \mathbf{E}(\mathbf{r}_d)|^2 / |\mathbf{p}_d \cdot \mathbf{E}_{\mathrm{in}}(\mathbf{r}_d)|^2$. With the help of the Q matrices of the individual layers, one can obtain the EM field at any point and thus evaluate η_{exc} for a given excitation frequency and orientation of the elementary dipole.

Since in fluorescence there is no coherence between excitation and emission, we can treat these two processes independently. In the spontaneous emission process, which will concern us here, the excited molecule is considered as a classical electric dipole and constitutes the source. An electric dipole moment $\mathbf{p}_d$ at point $\mathbf{r}_d$ in a homogeneous medium with (relative) permittivity and permeability ϵ and μ, respectively, oscillating with an angular frequency ω that is different in general from the excitation frequency, induces an external polarization field $\mathbf{P}(\mathbf{r}, t) = \mathrm{Re}[\mathbf{p}_d \delta(\mathbf{r} - \mathbf{r}_d) \exp(-i\omega t)]$. The EM field produced by this oscillating dipole has the same frequency ω, and its spatial component is obtained from Maxwell equations

$$\frac{c^2}{\epsilon\mu} \nabla \times \nabla \times \mathbf{E}_d(\mathbf{r}) - \omega^2 \mathbf{E}_d(\mathbf{r}) = \frac{\omega^2}{\epsilon\epsilon_0} \mathbf{p}_d \delta(\mathbf{r} - \mathbf{r}_d)$$
$$\mathbf{H}_d(\mathbf{r}) = \frac{-i}{\omega\mu\mu_0} \nabla \times \mathbf{E}_d(\mathbf{r}), \qquad \text{(A1)}$$

where ϵ_0, μ_0 are the vacuum permittivity and permeability, respectively, and $c \equiv 1/\sqrt{\epsilon_0 \mu_0}$ is the velocity of light. The first of Eqs. (A1) is an inhomogeneous differential equation and can be readily solved by the Green's function method. We obtain

$$\mathbf{E}_d(\mathbf{r}) = -\frac{\omega^2}{\epsilon\epsilon_0} \mathbf{G}(\mathbf{r}, \mathbf{r}_d) \mathbf{p}_d, \qquad \text{(A2)}$$

where $\mathbf{G}$ is the dyadic Green's function of the homogeneous host medium [37], which satisfies the equation

$$\frac{c^2}{\epsilon\mu} \nabla \times \nabla \times \mathbf{G}(\mathbf{r}, \mathbf{r}') - \omega^2 \mathbf{G}(\mathbf{r}, \mathbf{r}') = -\mathbf{I}\delta(\mathbf{r} - \mathbf{r}'), \qquad \text{(A3)}$$

$\mathbf{I}$ being the 2×2 unit matrix. $\mathbf{G}$ can be expanded into vector plane waves of wave number $q = \omega\sqrt{\epsilon\mu}/c$ as follows [37]:

$$\mathbf{G}(\mathbf{r}, \mathbf{r}') = -\frac{i\epsilon\mu}{8\pi^2 c^2} \int \mathrm{d}^2 q_{\parallel} \frac{e^{i\mathbf{q}^{\pm} \cdot (\mathbf{r} - \mathbf{r}')}}{\sqrt{q^2 - q_{\parallel}^2}} \sum_{p=1}^{2} \hat{\mathbf{e}}_p(\mathbf{q}^{\pm}) \hat{\mathbf{e}}_p(\mathbf{q}^{\pm}), \qquad \text{(A4)}$$

where $\mathbf{q}^{\pm} \equiv \mathbf{q}_{\parallel} \pm \sqrt{q^2 - q_{\parallel}^2} \hat{\mathbf{e}}_z$ corresponds to $z > z'$ (plus sign) and $z < z'$ (minus sign). The above expansion of the dyadic Green's function involves plane waves of any $\mathbf{q}_{\parallel}$. However only waves with $q_{\parallel} < q$ constitute propagating waves. When $q_{\parallel} > q$, we have evanescent waves and the corresponding unit vectors $\hat{\mathbf{e}}_1$, $\hat{\mathbf{e}}_2$ become complex, but they are still orthonormal: $\hat{\mathbf{e}}_p \cdot \hat{\mathbf{e}}_{p'} = \delta_{pp'}$, $p, p' = 1, 2$.

According to Eqs. (A2) and (A4), the electric field produced by the dipole emitter can be expanded into vector plane waves propagating or decaying along the positive z direction for $z > z_d$, i.e., on the right of the dipole, and vector plane waves propagating or decaying along the negative z direction for $z < z_d$, i.e., on the left of the dipole, as follows:

$$\mathbf{E}_d(\mathbf{r}) = \int \frac{\mathrm{d}^2 q_{\parallel}}{(2\pi q)^2} e^{i\mathbf{q}^{\pm} \cdot (\mathbf{r} - \mathbf{r}_d)} \sum_{p=1}^{2} E_{d;p}^{\pm} \hat{\mathbf{e}}_p(\mathbf{q}^{\pm}), \qquad \text{(A5)}$$

where the plus (minus) sign holds for $z > z_d$ ($z < z_d$) and

$$E_{d;p}^{\pm} = \frac{iq^4 p_d}{2\epsilon\epsilon_0 \sqrt{q^2 - q_{\parallel}^2}} \hat{\mathbf{e}}_p(\mathbf{q}^{\pm}) \cdot \hat{\mathbf{p}}_d. \qquad \text{(A6)}$$

Scattering by the multilayer slabs on both sides of the dipole gives rise to a secondary field, so that the total field is given by the primary field produced by the oscillating dipole plus the secondary field. Using the Q matrices of the multilayer slabs on the right (R) and left (L) of the dipole, one can take into account all multiple-scattering events and write the components of the total field that propagate or decay along the positive (+) and negative (−) z direction, in the layer where the dipole is implanted in, as follows:

$$\begin{aligned} E_{R;p}^{+} &= E_{d;p}^{+} + Q_{L;p}^{\mathrm{II}} Q_{R;p}^{\mathrm{III}} E_{d;p}^{+} + Q_{L;p}^{\mathrm{II}} Q_{R;p}^{\mathrm{III}} Q_{L;p}^{\mathrm{II}} Q_{R;p}^{\mathrm{III}} E_{d;p}^{+} + \cdots \\ &\quad + Q_{L;p}^{\mathrm{II}} E_{d;p}^{-} + Q_{L;p}^{\mathrm{II}} Q_{R;p}^{\mathrm{III}} Q_{L;p}^{\mathrm{II}} E_{d;p}^{-} \\ &\quad + Q_{L;p}^{\mathrm{II}} Q_{R;p}^{\mathrm{III}} Q_{L;p}^{\mathrm{II}} Q_{R;p}^{\mathrm{III}} Q_{L;p}^{\mathrm{II}} E_{d;p}^{-} + \cdots \\ &= (1 - Q_{L;p}^{\mathrm{II}} Q_{R;p}^{\mathrm{III}})^{-1} (E_{d;p}^{+} + Q_{L;p}^{\mathrm{II}} E_{d;p}^{-}), \end{aligned} \qquad \text{(A7)}$$

$$E_{R;p}^{-} = Q_{R;p}^{\mathrm{III}} E_{R;p}^{+} \qquad \text{(A8)}$$

on the right side of the dipole and

$$\begin{aligned} E_{L;p}^{-} &= E_{d;p}^{-} + Q_{R;p}^{\mathrm{III}} Q_{L;p}^{\mathrm{II}} E_{d;p}^{-} + Q_{R;p}^{\mathrm{III}} Q_{L;p}^{\mathrm{II}} Q_{R;p}^{\mathrm{III}} Q_{L;p}^{\mathrm{II}} E_{d;p}^{-} + \cdots \\ &\quad + Q_{R;p}^{\mathrm{III}} E_{d;p}^{+} + Q_{R;p}^{\mathrm{III}} Q_{L;p}^{\mathrm{II}} Q_{R;p}^{\mathrm{III}} E_{d;p}^{+} \\ &\quad + Q_{R;p}^{\mathrm{III}} Q_{L;p}^{\mathrm{II}} Q_{R;p}^{\mathrm{III}} Q_{L;p}^{\mathrm{II}} Q_{R;p}^{\mathrm{III}} E_{d;p}^{+} + \cdots \\ &= (1 - Q_{R;p}^{\mathrm{III}} Q_{L;p}^{\mathrm{II}})^{-1} (E_{d;p}^{-} + Q_{R;p}^{\mathrm{III}} E_{d;p}^{+}), \end{aligned} \qquad \text{(A9)}$$

$$E^{+}_{L;p} = Q^{\mathrm{II}}_{L;p} E^{-}_{L;p} \tag{A10}$$

on the left side of the dipole. It should be noted that in the above equations all Q matrices refer to plane waves in the region of the dipole that are expanded with respect to the same point $\mathbf{r}_d$.

The rate at which the emitting dipole loses its energy is defined as the net outflow of energy from two infinite surfaces, parallel to the x-y plane, in the layer where the dipole is implanted in: one on the right and one on the left of the dipole. Integrating the normal component of the Poynting vector over these surfaces, we obtain for the power flow to the right of the dipole

$$P_R = \frac{1}{8\pi^2 q^5}\sqrt{\frac{\epsilon\epsilon_0}{\mu\mu_0}}\int \mathrm{d}^2 q_{\parallel} \sum_{p=1}^{2} [|E^{+}_{R;p}|^2 - |E^{-}_{R;p}|^2] \times \mathrm{Re}\sqrt{q^2 - q_{\parallel}^2} - 2\,\mathrm{Im}[E^{+}_{R;p} E^{-*}_{R;p}]\mathrm{Im}\sqrt{q^2 - q_{\parallel}^2} \tag{A11}$$

and a similar expression for the power flow to the left of the dipole P_L, which can be obtained from Eq. (A11) by replacing $E^{+}_{R;p}$ by $E^{-}_{L;p}$ and $E^{-}_{R;p}$ by $E^{+}_{L;p}$. We note that positive (negative) sign of $P_{R(L)}$ means energy flow directed away from (towards) the dipole. The first term in Eq. (A11) involves only propagating waves ($q > q_{\parallel}$) and is clearly related to the transfer of energy by way of the far field of the dipole, while the last term involves only evanescent waves ($q > q_{\parallel}$) and represents energy transfer through the near field.

A certain fraction of the power emitted by the dipole is dissipated as Joule heating in the surrounding absorbing layers (nonradiative decay process). The rest of the power is radiated away in the outer host medium or transferred to possible guided modes of the multilayer slabs on both sides of the dipole. The total energy flow radiated in the outer host medium is evaluated by integrating the normal component of the Poynting vector over two infinite x-y planes: one on the right and one on the left of the whole multilayer structure. We obtain

$$P^{\mathrm{out}}_{R} = \frac{1}{8\pi^2 q^5}\sqrt{\frac{\epsilon\epsilon_0}{\mu\mu_0}}\int \mathrm{d}^2 q_{\parallel} \sum_{p=1}^{2} |E^{\mathrm{out}}_{R;p}|^2 \mathrm{Re}\sqrt{q^2 - q_{\parallel}^2} \tag{A12}$$

and a similar expression for P^{out}_{L} with $E^{\mathrm{out}}_{L;p}$ in place of $E^{\mathrm{out}}_{R;p}$, where $E^{\mathrm{out}}_{R;p} = Q^{\mathrm{I}}_{R;p} E^{+}_{R;p}$ and $E^{\mathrm{out}}_{L;p} = Q^{\mathrm{IV}}_{L;p} E^{-}_{L;p}$. Energy conservation implies that the power transferred into possible guided modes and Joule heating of the multilayer slabs on the right and left of the dipole is given by $P_{R(L)} - P^{\mathrm{out}}_{R(L)}$.

As pointed out in [15], for lossless dielectric layers, the integrands in Eq. (A11) have poles at the eigenmodes of the multilayer slab. To overcome this problem, we included a small imaginary part (10^{-4}) to the dielectric function, excluding the regions of the emitter, which ensures fast convergence of the integrals involved and accurate results [15]. This approach is simple to implement and, using an adaptive grid method, we obtain rapid convergence. At the same time, the method can be generalized in a straightforward manner to layered structures where the component layers are not homogeneous but have the same two-dimensional periodicity [34,35].

In the absence of any object in the homogeneous host medium, the radiation power emitted by the dipole can be calculated directly from Eq. (A11) noting that, in this case, there is no secondary field. After some straightforward algebra, we recover the well-known result

$$P_{0r} = \frac{c q^4 p_d^2}{12\pi\epsilon\epsilon_0\sqrt{\epsilon\mu}}. \tag{A13}$$

The total decay rate of the emitter in the host medium, in absence of the multilayer structure, is the sum of the radiative and nonradiative decay rates, Γ_{0r} ($= P_{0r}/\hbar\omega$) and $\Gamma_{0\mathrm{nr}}$, respectively. The latter accounts for intrinsic nonradiative decay mechanisms of the molecule, such as multiphoton processes, direct electron-transfer processes, etc., and does not depend on the environment. The intrinsic quantum yield of the emitter is defined as $q_0 = \Gamma_{0r}/(\Gamma_{0r} + \Gamma_{0\mathrm{nr}})$. The presence of the multilayer structure introduces additional decay channels through absorptive losses and excitation of guided modes, and thus the quantum yield takes the form $q = \Gamma^{\mathrm{out}}/(\Gamma + \Gamma_{0\mathrm{nr}})$. Using the definition of q_0, this can be recast as

$$q = \frac{\Gamma^{\mathrm{out}}/\Gamma_{0r}}{\Gamma/\Gamma_{0r} + q_0^{-1} - 1} = \frac{P^{\mathrm{out}}/P_{0r}}{P/P_{0r} + q_0^{-1} - 1}, \tag{A14}$$

where $P = P_R + P_L$ and $P^{\mathrm{out}} = P^{\mathrm{out}}_R + P^{\mathrm{out}}_L$ and q_0 is a given quantity characteristic of the emitter.

The emitted power of a radiating dipole depends on its exact position and orientation. For randomly oriented dipole sources, an average over different dipole orientations has to be performed. The average emitted power, P_{av}, is given by $P_{\mathrm{av}} = 2P_{\parallel}/3 + P_{\perp}/3$, where $P_{\parallel}(P_{\perp})$ is the emitted power if the dipole oscillates parallel (normal) to the layers, and is normalized to the corresponding power emitted in a homogeneous environment. By assuming an emitter with a quantum efficiency equal to unity, the spontaneous emission enhancement is proportional to the normalized emitted power. In the case of incoherent emission from a distribution of light emitters, it is necessary to sum up the time-averaged power over the distribution of the elementary dipoles. In the case of coherent emission, the total electric field at some point has to be calculated from the contributions of the individual dipoles prior to the time-averaged power calculation.

ACKNOWLEDGMENTS

This work is supported by the European Commission Seventh Framework Programme (FP7) under the Future and Emerging Technologies (FET)-Open project TAILPHOX N 233883. E. Almpanis was supported by the National Center for Scientific Research (NCSR) "Demokritos" through a postgraduate fellowship.

REFERENCES

1. E. M. Purcell, "Spontaneous emission probabilities at radio frequencies," Phys. Rev. **69**, 681 (1946).
2. G. Björk, S. Machida, Y. Yamamoto, and K. Igeta, "Microcavity semiconductor laser with enhanced spontaneous emission," Phys. Rev. A **44**, 669–681 (1991).
3. A. M. Vredenberg, N. E. J. Hunt, E. F. Schubert, D. C. Jacobson, J. M. Poate, and G. J. Zydzik, "Controlled atomic spontaneous

emission from Er3+ in a transparent Si/SiO_2 microcavity," Phys. Rev. Lett. **71**, 517–520 (1993).
4. S. R. J. Brueck, V. A. Smagley, and P. G. Eliseev, "Radiation from a dipole embedded in a multilayer slab," Phys. Rev. E **68**, 036608 (2003).
5. M. Wubs, L. G. Suttorp, and A. Lagendijk, "Spontaneous-emission rates in finite photonic crystals of plane scatterers," Phys. Rev. E **69**, 016616 (2004).
6. A. S. Sánchez and P. Halevi, "Spontaneous emission in one-dimensional photonic crystals," Phys. Rev. E **72**, 056609 (2005).
7. X. W. Chen, W. C. H. Choy, and S. He, "Efficient and rigorous modeling of light emission in planar multilayer organic light-emitting diodes," J. Disp. Technol. **3**, 110–117 (2007).
8. M. Notomi, "Manipulating light with strongly modulated photonic crystals," Rep. Prog. Phys. **73**, 096501 (2010).
9. H. Schniepp and V. Sandoghdar, "Spontaneous emission of europium ions embedded in dielectric nanospheres," Phys. Rev. Lett. **89**, 257403 (2002).
10. S. J. Dewhurst, D. Granados, D. J. P. Ellis, A. J. Bennett, R. B. Patel, I. Farrer, D. Anderson, G. A. C. Jones, D. A. Ritchie, and A. J. Shields, "Slow-light-enhanced single quantum dot emission in a unidirectional photonic crystal waveguide," Appl. Phys. Lett. **96**, 031109 (2010).
11. V. S. C. Manga Rao and S. Hughes, "Single quantum dot spontaneous emission in a finite-size photonic crystal waveguide: proposal for an efficient on chip single photon gun," Phys. Rev. Lett. **99**, 193901 (2007).
12. G. W. Ford and W. H. Weber, "Electromagnetic interactions of molecules with metal surfaces," Phys. Rep. **113**, 195–287 (1984).
13. C. Creatore and L. C. Andreani, "Quantum theory of spontaneous emission in multilayer dielectric structures," Phys. Rev. A **78**, 063825 (2008).
14. N. H. Liu, J. P. Xu, and S. Y. Zhu, "Non-Markovian dynamic evolution of spontaneous emission decay of a two-level atom embedded in one-dimensional photonic crystals," Phys. Rev. B **74**, 075314 (2006).
15. Y. C. Jun, R. M. Briggs, H. A. Atwater, and M. L. Brongersma, "Broadband enhancement of light emission in silicon slot waveguides," Opt. Express **17**, 7479–7490 (2009).
16. J. H. Wülbern, A. Petrov, and M. Eich, "Electro-optical modulator in a polymer infiltrated silicon slotted photonic crystal waveguide heterostructure resonator," Opt. Express **17**, 304–313 (2009).
17. M. Brunstein, R. Braive, R. Hostein, A. Beveratos, I. Robert-Philip, I. Sagnes, T. J. Karle, A. M. Yacomotti, J. A. Levenson, V. Moreau, G. Tessier, and Y. de Wilde, "Thermo-optical dynamics in an optically pumped photonic crystal nano-cavity," Opt. Express **17**, 17118–17129 (2009).
18. D. A. Fuhrmann, S. M. Thon, H. Kim, D. Bouwmeester, P. M. Petroff, A. Wixforth, and H. J. Krenner, "Dynamic modulation of photonic crystal nanocavities using gigahertz acoustic phonons," Nat. Photon. **5**, 605–609 (2011).
19. C. Brüggemann, A. V. Akimov, A. V. Scherbakov, M. Bombeck, C. Schneider, S. Höfling, A. Forchel, D. R. Yakovlev, and M. Bayer, "Laser mode feeding by shaking quantum dots in a planar microcavity," Nat. Photon. **6**, 30–34 (2012).
20. A. V. Scherbakov, T. Berstermann, A. V. Akimov, D. R. Yakovlev, G. Beaudoin, D. Bajoni, I. Sagnes, J. Bloch, and M. Bayer, "Ultrafast control of light emission from a quantum-well semiconductor microcavity using picosecond strain pulses," Phys. Rev. B **78**, 241302(R) (2008).
21. H. Lin, C. H. Lin, W. C. Lai, Y. S. Lee, S. D. Lin, and W. H. Chang, "Stress tuning of strong and weak couplings between quantum dots and cavity modes in microdisk microcavities," Phys. Rev. B **84**, 201301 (2011).
22. S. Völk, F. J. R. Schülein, F. Knall, D. Reuter, A. D. Wieck, T. A. Truong, H. Kim, P. M. Petroff, A. Wixforth, and H. J. Krenner, "Enhanced sequential carrier capture into individual quantum dots and quantum posts controlled by surface acoustic waves," Nano Lett. **10**, 3399–3407 (2010).
23. J. B. Kinzel, D. Rudolph, M. Bichler, G. Abstreiter, J. J. Finley, G. Koblmüller, A. Wixforth, and H. J. Krenner, "Directional and dynamic modulation of the optical emission of an individual GaAs nanowire using surface acoustic waves," Nano Lett. **11**, 1512–1517 (2011).
24. J. M. M. de Lima, R. Hey, and P. V. Santos, "Active photonic crystals based on surface acoustic waves," Appl. Phys. Lett. **83**, 2997–2999 (2003).
25. J. R. Zurita-Sánchez, P. Halevi, and J. C. Cervantes-González, "Reflection and transmission of a wave incident on a slab with a time-periodic dielectric function $\epsilon(t)$," Phys. Rev. A **79**, 053821 (2009).
26. N. V. Budko, "Electromagnetic radiation in a time-varying background medium," Phys. Rev. A **80**, 053817 (2009).
27. J. R. Zurita-Sánchez and P. Halevi, "Resonances in the optical response of a slab with time-periodic dielectric function $\epsilon(t)$," Phys. Rev. A **81**, 053834 (2010).
28. M. Eichenfeld, J. Chan, R. M. Camacho, K. J. Vahala, and O. Painter, "Optomechanical crystals," Nature **462**, 78–82 (2009).
29. J. Chan, T. P. Mayer Alegre, A. H. Safavi-Naeini, J. T. Hill, A. Krause, S. Gröblacher, M. Aspelmeyer, and O. Painter, "Laser cooling of a nanomechanical oscillator into its quantum ground state," Nature **478**, 89–92 (2011).
30. S. Weis, R. Rivière, S. Deléglise, E. Gavartin, O. Arcizet, A. Schliesser, and T. J. Kippenberg, "Optomechanically induced transparency," Science **330**, 1520–1523 (2010).
31. I. E. Psarobas, N. Papanikolaou, N. Stefanou, B. Djafari-Rouhani, B. Bonello, and V. Laude, "Enhanced acousto-optic interactions in a one-dimensional phoxonic cavity," Phys. Rev. B **82**, 174303 (2010).
32. N. Papanikolaou, I. E. Psarobas, N. Stefanou, B. Djafari-Rouhani, B. Bonello, and V. Laude, "Light modulation in phoxonic nanocavities," Microelectron. Eng. **90**, 155–158 (2012).
33. J. R. Gell, M. B. Ward, R. J. Young, R. M. Stevenson, P. Atkinson, D. Anderson, G. A. C. Jones, D. A. Ritchie, and J. Shields, "Modulation of single quantum dot energy levels by a surface-acoustic-wave," Appl. Phys. Lett. **93**, 081115 (2008).
34. N. Stefanou, V. Yannopapas, and A. Modinos, "Heterostructures of photonic crystals: frequency bands and transmission coefficients," Comput. Phys. Commun. **113**, 49–77 (1998).
35. N. Stefanou, V. Yannopapas, and A. Modinos, "MULTEM2: A new version of the program for transmission and band-structure calculations of photonic crystals," Comput. Phys. Commun. **132**, 189–196 (2000).
36. R. Sainidou, N. Stefanou, I. E. Psarobas, and A. Modinos, "A layer-multiple-scattering method for phononic crystals and heterostructures of such," Comput. Phys. Commun. **166**, 197–240 (2005).
37. W. C. Chew, *Waves and Fields in Inhomogeneous Media* (IEEE Press, 1995).